Optical NDE Methods for Ceramic Thermal Barrier Coatings

**William A. Ellingson, Robert J. Visher, Rachel S. Lipanovich,
and Christopher M. Deemer**
Energy Technology Division
Argonne National Laboratory
Argonne, IL 60439

November 2005

_____

Optical NDE Methods for Ceramic Thermal Barrier Coatings

William A. Ellingson, Robert J. Visher, Rachel S. Lipanovich, and Christopher M. Deemer

Energy Technology Division, Argonne National Laboratory, Argonne, IL 60439

ABSTRACT

Thermal barrier coatings (TBCs), usually consisting of yttria-stabilized zirconia (YSZ), are used in gas turbine engines to reduce the operating temperature of the superalloy base metal. A typical coating system is composed of a superalloy substrate, a bond coat, and the top coat or TBC. In high-performance propulsion turbines and low-emission electric power gas turbine TBCs are critical because if they are lost during operation, damage to the substrate material may occur. Reliable non-contact, nondestructive methods are required to monitor the condition of the TBC and predict coating failure. Several nondestructive evaluation (NDE) methods are in various stages of development for determining the status of these critical TBCs. Optical NDE methods take advantage of the fact that TBCs are optically translucent. As a result, surfaces within and below the TBC can be examined using appropriate optical wavelengths. Optical NDE methods presently under study include luminescence spectroscopy, laser back scatter, optical coherence tomography, thermal imaging, and mid-infrared back scatter. The choice of the NDE method depends, to some extent, upon the particular type of TBC. Most TBCs are applied with electron-beam physical vapor deposition (EB-PVD) or air plasma spraying (APS). This paper discusses the various NDE techniques and provides some experimental results.

INTRODUCTION

Thermal barrier coatings (TBCs) [1-2] are critical for increasing gas-firing temperatures in both stationary power generation and propulsion turbine engines.   An engine with TBC-coated components will have a service life significantly longer than an engine with uncoated components [3]. Failure of a TBC could lead to a costly unplanned outage and could lead to catastrophic events.   It is therefore necessary to monitor the condition of the TBC so as to avoid such failures and, if possible, to provide pre-cursor information that would suggest whether spallation is imminent.   Several investigators [4-8] have shown that failure of the coatings depends upon the coating type, EB-PVD or APS.   Detection of spalled regions or regions where spallation might occur in the near future, therefore, depends upon the coating type. There is also a need to determine changes in the thermal conductivity of these TBC materials. Such changes can arise from diffusion of combustion constituents into the coating, especially for turbines burning "dirty" fuels. Further, conductivity can change due to microstructural changes in the TBC, such as in-situ sintering. From the NDE point of view, the microstructural differences between an EB-PVD and APS TBC are significant. An EB-PVD coating has a better-defined columnar microstructure [1-2] and is less optically scattering than the "splat" microstructure of an APS coating [1-2]. NDE technologies that can accommodate these microstructural differences and measure the desired TBC parameters are important for ensuring the long-term reliable operation of advanced, high-efficiency, low-emission gas turbines.

In an EB-PVD TBC system, a thermally grown oxide (TGO) layer, typically on the order of 1-2 µm thick, forms at the TBC/bond coat interface when the TBC is applied. The thickness of the TGO is known to increase as a function of time at operating temperature (i.e., number of

thermal cycles) for both EB-PVD and APS TBCs. The greater thickness of the TGO layer has been shown [4-7] to increase stress levels at the TBC/bond coat interface to such levels that eventual spallation occurs. This stress is relieved by a "rumpling" or "rippling" of the TGO [3], which has been related to failure [6,7].   Subsurface defects, such as cracks, within the TBC layer are also of concern as they can also lead to coating failure [5-8].

Several NDE approaches have been examined for studying TBCs. For delamination detection, pre-spall prediction, and thickness measurements, NDE approaches included use of eddy currents [9], electrically conducting fluids [10-11], microwaves [12], thermal imaging [13], and laser-based optics [14-16].   Optical methods, either thermal or laser-based, show the most promise, and several methods are under various stages of development. Most optical methods focus on the condition of the TGO layer. One laser-based method that has received significant attention for EB-PVD coatings is luminescence spectroscopy [17-20]. In this method, a laser excites Cr^{3+} ions in the TGO whose concentration has been correlated to the stress levels in the TGO. The fluorescence response is a spectral shift, and the size of that shift and the shape of the spectra response curve are important to the analysis. At the present time, this method may have limitations for thick TBCs applied with APS. A second method, based on thermal imaging technology, is being explored for thick APS coatings. It is referred to as mid-infrared (IR) back reflectance and has been developed by Eldridge at NASA [21]. In this method, steady-state mid-IR heating sources are placed on the IBC side of the test sample to stimulate the interface layer, or TGO, and the resulting back reflectance is captured by an IR camera with high frame rate and 3-5 µm band pass. Correlations have been established between progression of delamination cracks, which has been related to pre-spall condition, and the IR back reflectance.

Clearly, more conventional thermal imaging [13] using state-of-the-art focal-plane array IR cameras can provide information about delaminated regions of TBCs. Recent work at Argonne National Laboratory has shown that, in addition to detection of delaminated regions, detection of plugged internal cooling passages is also possible.

Another laser-based optical method under development for delamination detection and for pre-spallation prediction is elastic optical scattering (EOS) [21]. This method is being developed at Argonne National Laboratory [14-16]. In this method, low-power (< 35 mW) polarized laser light penetrates to the TGO interface, where the light is back scattered. Calculations with theoretical model based on electromagnetic scattering principles have been compared to experiments [22].

Thickness uniformity of the TBCs is yet another characteristic of importance [23].   The temperature drop across the TBC is dependent upon the thickness, especially if the thermal conductivity is uniform.   A recent laser-based technology under study is optical coherence tomography (OCT) [24,25].   In this technology, which is capable of direct thickness measurements, a low-power laser is combined with fiber optics and an interferometer, such that cross-sectional images are obtained. These cross-sectional images can be either normal to the local surface, yielding direct thickness measurement, or parallel to the surface, yielding tomography sectional planes of significant detail regarding sizes of features in that plane. While this technology is still very much in development, there has been recent progress. We next describe these NDE optical methods in more detail and summarize experimental results obtained with them.

LUMINESCENCE SPECTROSCOPY

Luminescence spectroscopy, sometimes also called "piezospectroscopy," was pioneered in 1996 by David Clarke [17-19] relative to the study of TBCs. Several recent papers [26,27] have been written about luminescence spectroscopy, and the reader is encouraged to review these. In this NDE method, a laser is incident to the top TBC surface and, because of the optical translucency, can penetrate to the TGO. The TGO is mainly aluminum oxide and contains a few Cr^+ ions. When stimulated by the incident laser beam, the chromium ions will luminesce in two spectral lines, R1 and R2. The reflected light is detected by an optical microscope that is connected to a spectrometer.   The output of the spectrometer is sent to a CCD device connected to a computer. The TBC can be scanned with the input laser and the detecting microscope. Since the microscope is used in the detector train, the spot size that one can use can be less than 5 µm. When no strain is in the TGO, the R1 line emitted is 1.79 eV, and R2 will emit at 1.794 eV. However, when there is a strain in the TGO, the luminescence on these lines undergoes a spectral shift. Figure 1 shows the change in the emitted spectra for a stress-free TGO and a stressed coating. Efforts are underway to commercialize this type of device.
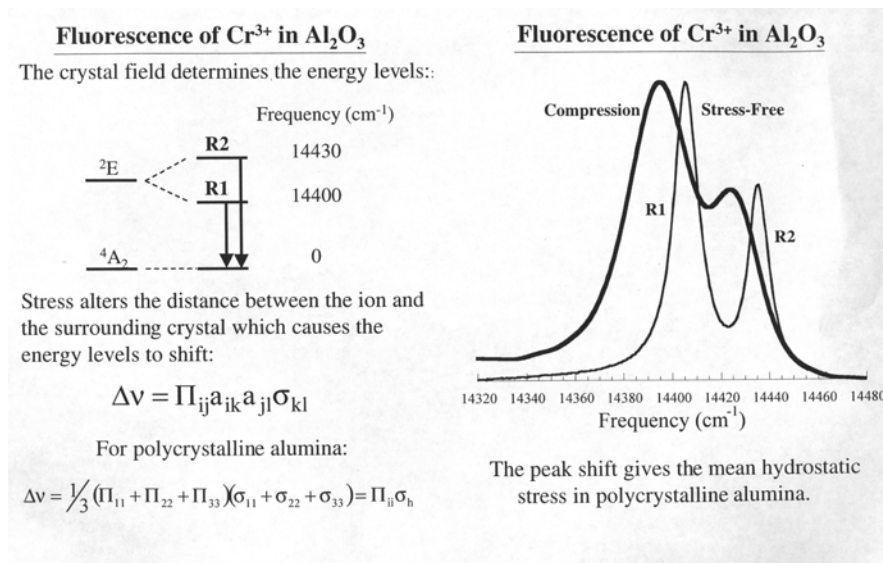

Fig. 1. Schematic diagrams of how energy levels and spectra
of Cr^+ ions change with stress level.

MID-IR BACK REFLECTANCE SPECTROSCOPY

In the mid-IR reflectance spectroscopy method, developed by Eldridge [21], steady-state heating sources with a high IR-output energy band are placed on the TBC side, as is an infrared camera with highly selected optical band pass detection (3-5 µm). This NDE method has been developed primarily to examine thick APS coatings as the luminescence spectroscopy method has had problems with thick TBCs. As shown in Fig. 2, Eldridge et al. [21] found that the reflectance increases as the damage level at the TBC/TGO interface increases. Eldridge has correlated the detected damage with SEM images, as shown in Fig. 3.
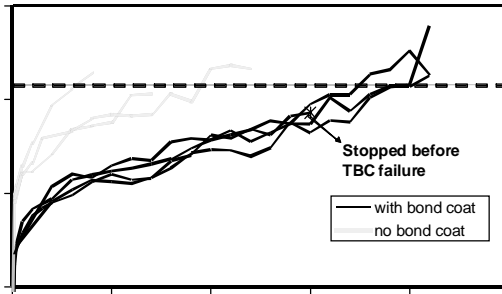
4

Fig. 2. Effect of furnace cycling on hemispherical reflectance at λ = 3.8 µm for TBC-coated specimens (~200-µm-thick) with and without bond coats (after Eldridge et al. [21]).
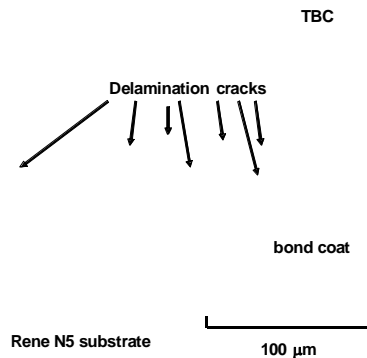

Fig. 3. SEM micrograph of TBC/bond coat interfacial region for TBC-coated specimen after 150 furnace cycles to 1163°C showing formation of delamination crack network [21].

INFRARED THERMAL IMAGING

A more common approach to detection of delaminations of TBCs has been to use focal-plane array infrared cameras that have high frame capture rates [13]. A typical setup is shown in Fig. 4.

Of interest to turbine blades with TBCs is the determination of whether or not the internal cooling passages have been plugged during any part of the processing. Figure 5a is a photograph of a typical turbine blade with a TBC applied. Notice the cooling holes on both the pressure side and the suction side of the blade.   These are integral to the internal cooling passages. Figure 5b shows that the one-sided thermal imaging can detect the open internal cooling channels. This IR image of an EB-PVD TBC was obtained by using a manifold with cold flowing air through the internal channels. Similar thermal imaging results can be obtained for APS TBCs, as indicated by Fig. 6.
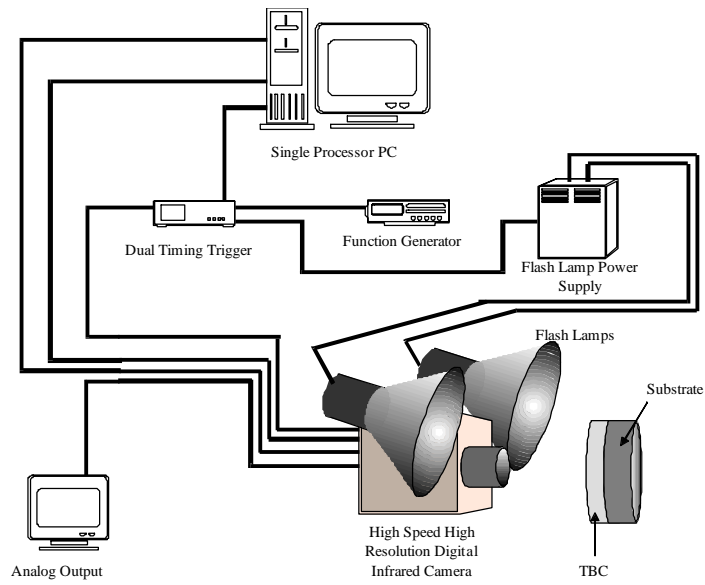
Fig. 4. Schematic diagram of one-sided thermal imaging setup for study of TBC.
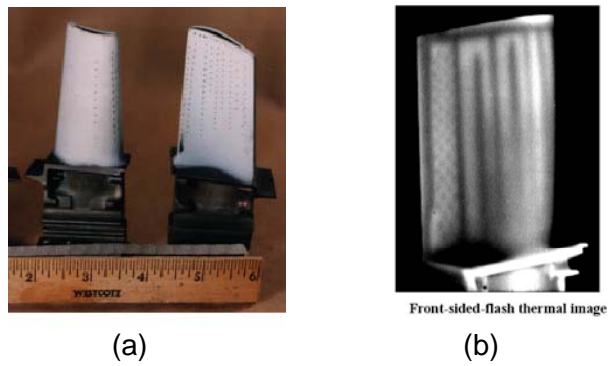

(a)   (b)

Fig. 5. Thermal imaging of turbine blade with EB-PVD TBC:
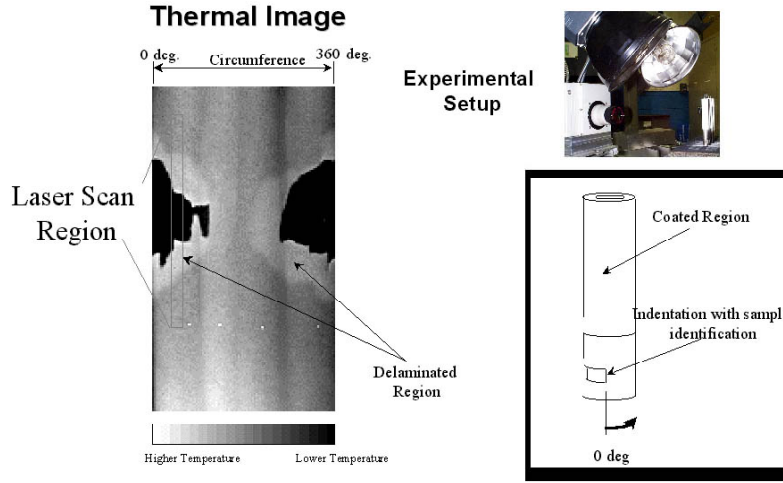(a) photographs, and (b) infrared image of turbine blade.

Fig. 6. Results of one-sided thermal imaging to detect disband on air-plasma-spray TBC.
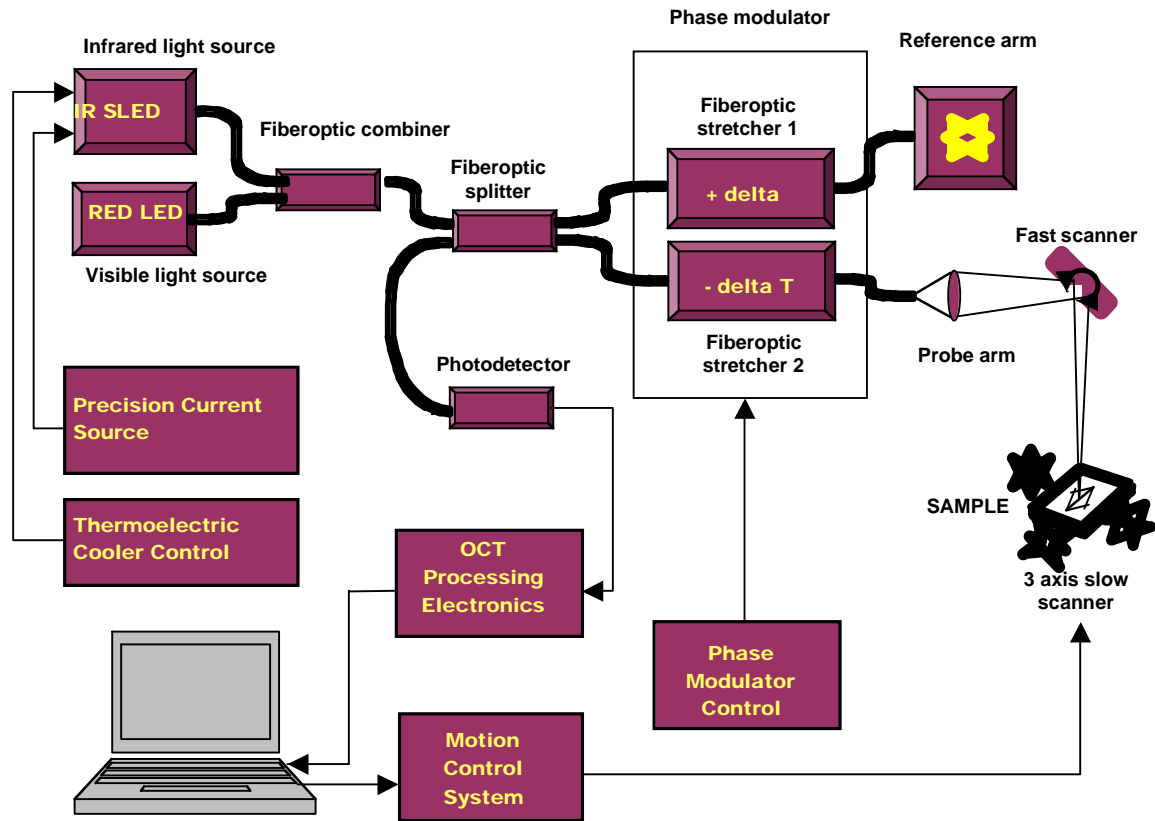
OPTICAL COHERENCE TOMOGRAPHY

Fig. 7. Block diagram of basic elements in OCT system.

Optical coherence tomography (OCT) has recently begun to be investigated as a tool for evaluating the condition of TBCs. This tomographic technique [24,25] is based on a Michelson interferometer. A block diagram of the OCT system used for this study is shown in Fig. 7. An advantage of this scanning system is the resolution in the image that is produced. The average OCT system can scan an object to a resolution of 5–15 μm.

Light from an optical source is split into two paths, a sample path and a reference path. Light in the reference path is reflected from a fixed-plane mirror, whereas light in the sample path is reflected from surface and subsurface features of the ceramic sample. The reflected light from the sample path will only be detected if it travels a distance that closely matches the distance traveled by the light in the reference path; this constraint incorporates depth resolution into the technique. Thus, data can be obtained from a cross-sectional plane perpendicular or parallel to the surface of the sample. Details of the experimental setup can be found in Visher et al. [22].

To demonstrate the application of this technology, a 25-mm-diameter button sample was prepared with a MCrAlY bond coat and EB-PVD TBC of yttria-stabilized zirconia (ysz). A bevel was then polished on the surface of the TBC, as shown in the cross-sectional schematic diagram in Fig. 8.
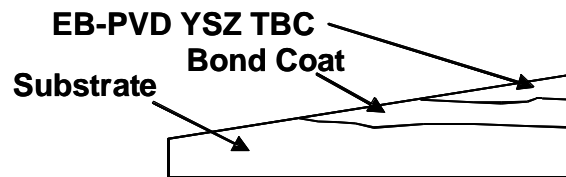

Fig. 8. Cross-sectional schematic diagram of TBC sample with polished bevel.

The Argonne OCT was used to obtain a cross-sectional image perpendicular to the top surface of the TBC. The resultant image, shown in Fig. 9a, reveals two strong reflections. The first reflection is from the top surface of the TBC itself; the second is from the TBC/bond coat interface from the point at which the TBC begins to cover the bond coat until the point at which the TBC is thick enough to attenuate the reflected signal enough to prohibit its detection.
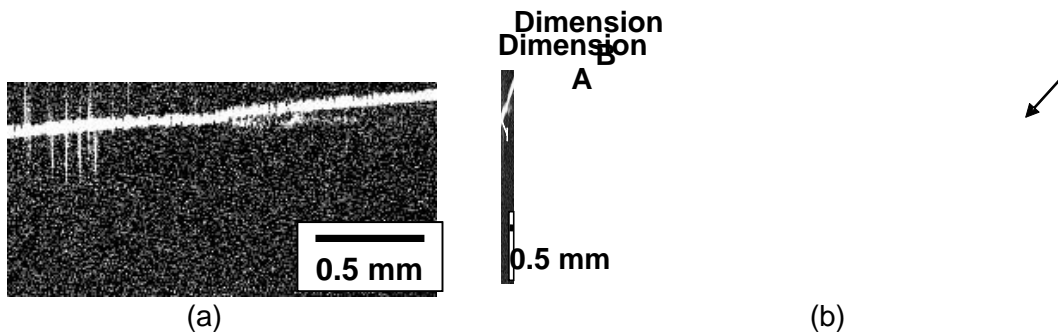

Fig. 9. (a) OCT cross-sectional image perpendicular to plane of TBC. (b) Same OCT image with dimensional markers for measurement of coating thickness. Note: measurements were taken from the middle of the thick white line visible in the image.

These two reflections can be used to measure the coating thickness. Cross-sectional optical micrographs are shown in Fig. 10. The TBC thickness was determined from both the 20X micrograph and the OCT image at the positions labeled "Dimension A" and "Dimension B" in Fig. 9b. These measurements are presented in Table 1.
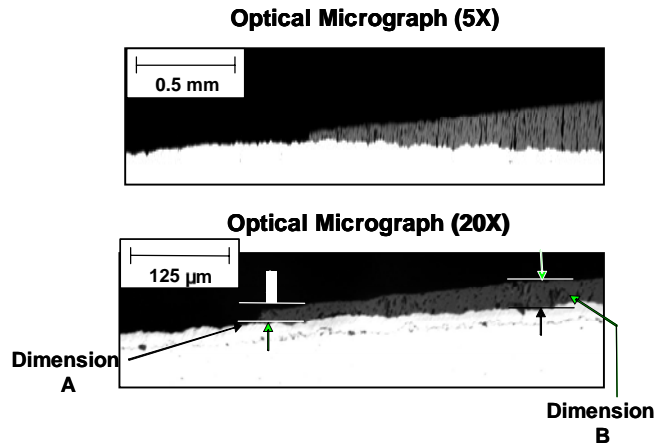

Fig. 10. Optical micrographs (5X and 20X) of polished cross section
of EB-PVD TBC sample with polished bevel.

Table 1. TBC coating thickness measurements from
optical micrograph and OCT image.

Source of Measurements	Dimension A	Dimension B
Micrograph	25 µm	44 µm
OCT	20 µm	50 µm

The OCT and micrograph measurements are quite close. It is important to note that the micrograph measurement required cutting the sample to obtain the cross section, whereas the OCT image and measurements were obtained without destroying the sample. At present, OCT technology utilizing superluminescent light-emitting diodes with > 1 µm wavelength is limited to penetration depths of <300 µm in TBCs. The scattering nature of the TBCs, combined with the OCT requirement for a high signal-to-noise ratio, is the current obstacle.

Figure 11 shows the results from applying OCT to an actual turbine blade with an EB-PVD TBC. As noted above, because of the highly scattering nature of the microstructures of the APS coatings, the use of OCT has been limited to EB-PVD coatings.
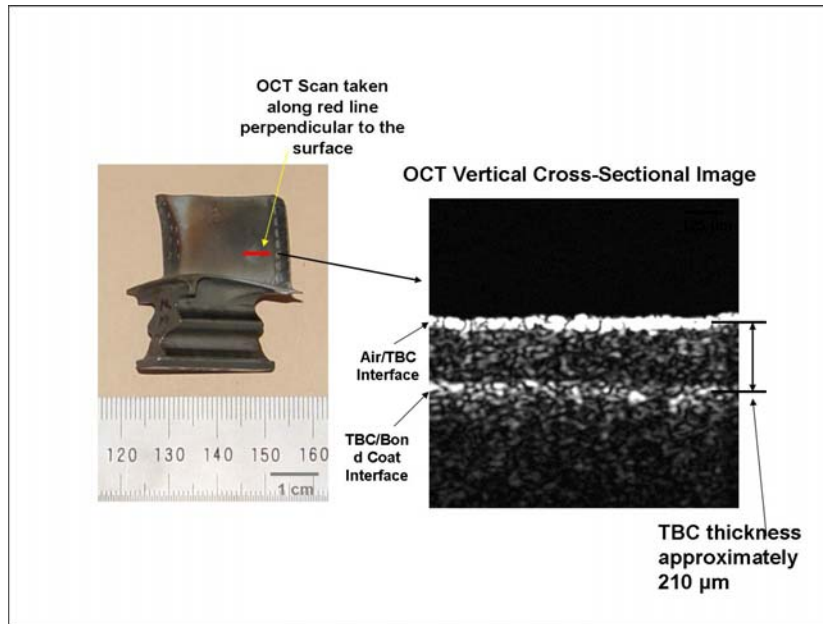
Fig. 11. Optical coherence tomography used to measure TBC thickness
on pressure side of EB-PVD coated turbine blade.

ELASTIC OPTICAL SCATTERING

The EOS technique [14-16] relies on polarized laser light to probe the sub-surface of an optically translucent material. The technique has been used to investigate thermal barrier coatings, specifically for health monitoring during isothermal heat-treatment testing.   The physical properties of ceramic materials are such that when a polarized laser beam is incident on the air/ceramic interface, a portion of the transmitted light will change polarization states, but the reflected light will not [21]. This property allows light scattered from subsurface defects and features to be measured while filtering out all other reflections.
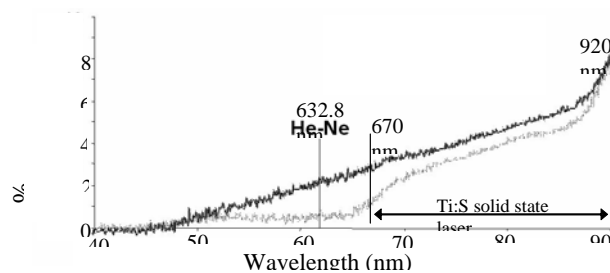

Fig. 12. Optical transmission of two free-standing YSZ coatings
applied by EB-PVD as a function of wavelength.

Figure 12 shows an optical transmission plot for a typical EB-PVD YSZ coating and demonstrates that TBCs have an optical translucency over a broad visible and near IR spectrum. The transmittance was measured for two free-standing EB-PVD TBC specimens of 350-µm thickness and different compositions. A similar test has been conducted with a free-standing APS TBC with 500-µm thickness and shows transmittance over a similar range but with a higher transmittance "peak" near the 632-nm wavelength of a He-Ne laser.

A change in the distribution of the backscatter light will occur when a feature is present that will sufficiently scatter the light.

A scanning process (see Fig. 13) is used to generate gray-scale images. Two different gray-scale images are generated. The first image is calculated from the sum of the measurements of Detectors A and B. The second image is calculated from the ratio of the measurement of Detector B to the measurement of Detector A.
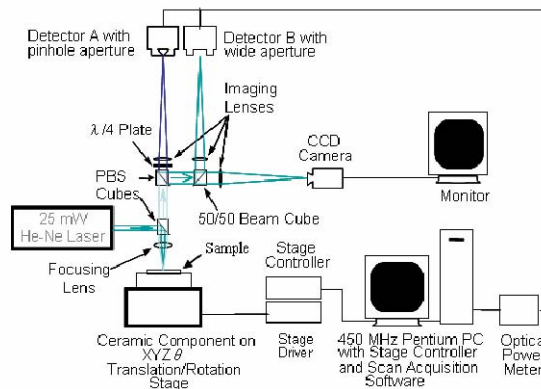

Fig. 13. Schematic of the elastic optical scattering experimental system
developed at Argonne National Laboratory.

The EOS method has been applied to two sets of 25-mm diameter button samples consisting of a superalloy substrate, MCrAlY bond coat, and YSZ TBC. The TBC on one set was applied by the EB-PVD method and was approximately 350-µm thick, while the TBC for the second set was applied using APS and was approximately 500-µm thick. The samples were subjected to thermal cycling until failure, and laser backscatter data were acquired at various intervals during the thermal cycling. A thermal cycle consisted of 50 min at 2075°F and 10 min cooling, with a ramp-up time to the temperature of about 8 min.

The EB-PVD sample set was investigated after exposure to 48, 96, 146, 171, and 191 thermal cycles. The laser backscatter images are shown in Fig. 14. The data acquired at 96 thermal cycles are not shown because of a data acquisition error.
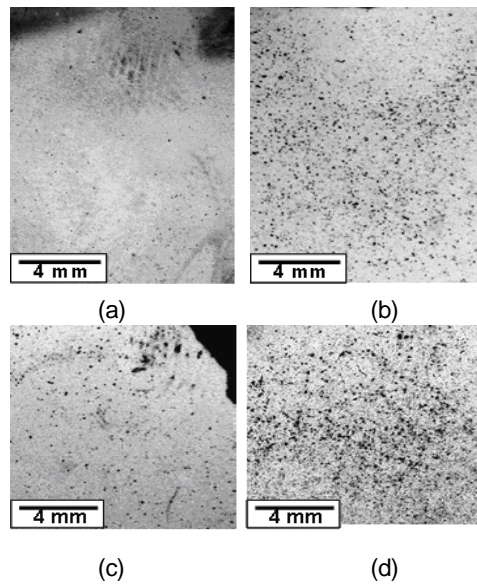
Fig. 14. Laser backscatter sum images for EB-PVD TBC sample 1A after
exposure to (a) 48, (b) 146, (c) 171, and (d) 191 thermal cycles.

The image size after 171 and 191 thermal cycles is smaller due to the spallation of the TBC.
The average detected power from the backscatter light is plotted as a function of the number of
thermal cycles in Fig. 15. The data indicate a significant increase in the total backscattered light
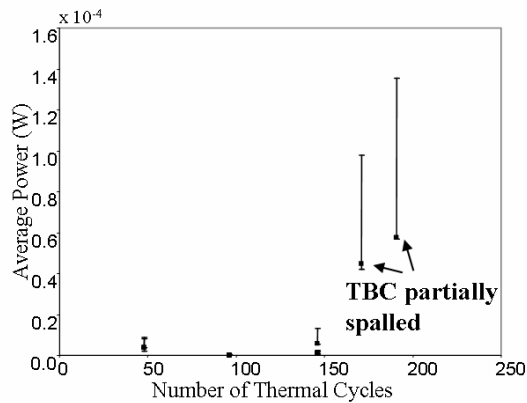power as the TBC approaches failure.

Fig. 15. Average detected light power from backscatter for EB-PVD
samples as a function of the number of thermal cycles.

Tests done using the APS samples with a 500-µm-thick TBC were thermal cycled until failure by
the same treatment as the EB-PVD samples. The EOS data were acquired in the as-processed
condition and after 233 and 326 thermal cycles. The final examination of these samples
occurred at failure, which was at 374 thermal cycles .The resulting laser backscatter sum
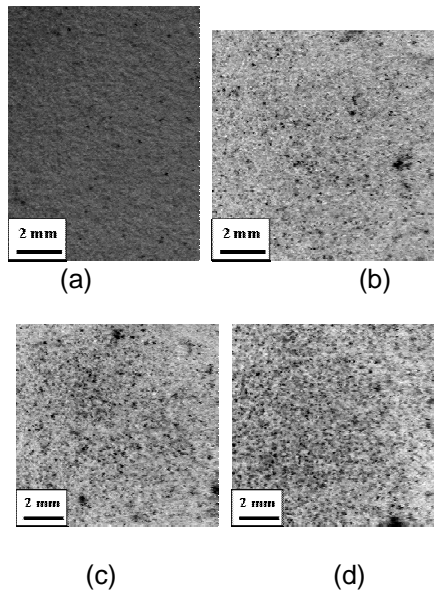images are shown in Fig. 16.

Fig. 16. Laser backscatter sum images from APS samples in the (a) as-processed condition
and after (b) 233, (c) 326, and (d) 374 thermal cycles.

The average power is plotted as a function of the number of thermal cycles for the APS samples in Fig.17. A similar increase in detected power is again observed as the sample approaches failure.
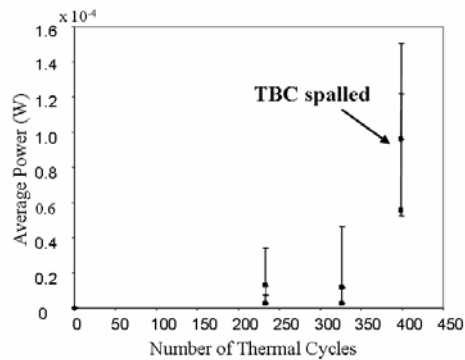

Fig. 17. Average detected reflected power value as a function
of the number of thermal cycles for APS TBC samples.

Others have noted [4-8] that the thickness of the TGO layer that forms at the TBC/bond coat interface could be a critical indicator of imminent coating failure [26-29].   To address the effect of the TGO thickness, 25-mm-diameter button samples were prepared by a similar method to that used for the earlier samples.   These samples were heat treated to produce a TGO of known thicknesses: 2, 5, 7, 9, 11, and 13 µm. Each of these samples was investigated by the laser backscatter method with a single 500-µm-thick APS TBC affixed to the TGO surface. The average detected power as a function of TGO thickness is shown in Fig. 18.
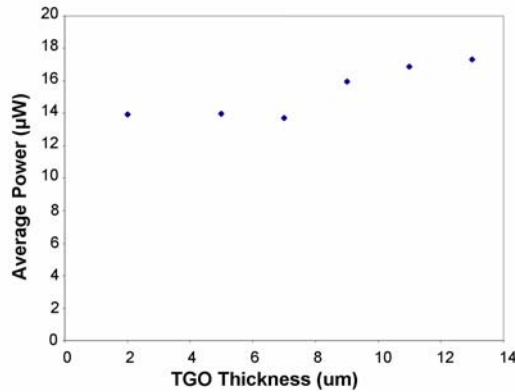
13

Fig. 18.   Average detected back-scattered-light power
as a function of TGO thickness with APS TBC.

A slight increase in the average power is observed as the TGO thickness increases above 6 µm. This finding is somewhat significant because this value is thought to be the point where critical thickness begins.

SUMMARY

Several optical NDE methods are under development to assess the condition or "health" of TBCs.   The application of a particular method depends to some extent upon the type of TBC, i.e., whether it is applied by EB-PVD or APS. It also depends upon whether one wishes to predict spallation or detect delamination. NDE method that can measure coating thickness is under development, as is a method that can assess changes in thermal conductivity. Yet to be determined is whether data acquired from these optical NDE methods would be affected by deposits caused by burning "dirty" fuels.

ACKNOWLEDGMENT

REFERENCES

1.   National Materials Advisory Board/National Research Council, "Coatings for High-Temperature Structural Materials," National Academy Press, Washington, DC (1996).

2.   Advisory Group for Aerospace Research and Development (AGARD)/NATO, "Thermal Barrier Coatings," AGARD report 823, North Atlantic Treaty Organization (1997).

3.   S.R. Choi, J.W. Hutchinson, and A.G. Evans, "Delamination of Multilayer Thermal Barrier Coatings," Mech. Mater. 31, 431-47 (1999).

4. A. M. Karlsson, and A. G. Evans, "Numerical Model for the Cyclic Instability of Thermally Grown Oxides in Thermal Barrier Coating Systems," Acta Materialia, 49(10), 1793-1804 (2001).

5. A. M. Karlsson, J. W. Hutchinson, and A. G. Evans, "The Displacement of the Thermally Grown Oxide in Thermal Barrier Coating Systems upon Temperature Cycling," Mat. Sci. Eng. A, 351 (1-2), 244-257 (2003).

6. A. M. Karlsson, J. W. Hutchinson, and A. G. Evans, "A Fundamental Model of Cyclic Instabilities in Thermal Barrier Systems," J. Mech. Phys. Sol., 50, 1565-89, (2002).

7. D. R. Mumm, and A. G. Evans, "On the Roles of Imperfections in the Failure of a Thermal Barrier Coating Made by Electron-Beam Physical Vapor Deposition," Acta Materialia, 48, 1815-27, (2000).

8. S. R. Choi, J. W. Hutchinson, and A. G. Evans, "Delamination of Multilayer Thermal Barrier Coatings," Mech. Mat., 31, 431-37 (1999).

9. N. Goldfine, A. Washabaugh, K. Walrath, P. Zombo, and R. Miller, "Conformable Eddy Current Sensors and Methods for Gas Turbine Inspection and Health Monitoring," Proc. Gas Turbine Materials Technology, eds., P. J. Maziasz, I. G. Wright, W. J. Brindley, J. Stringer, and C. O'Brien, pp. 105-114 (1998). Published by ASM International, Materials Park, OH.

10. S. Vishweswaraiah, B. Jayaraj, T. Du, V.H. Desai, and Y.H. Sohn, "Non-Destructive Microstructural Evaluation of Thermal Barrier Coatings by Electrochemical Impedance Spectroscopy," *proceedings of the 2003 International Thermal Spray Conference and Exposition,* ITSC 2003, eds. B.R. Marple and C. Moreau, ASM International, pp. 1487-1494 (2003).

11. B. Jayaraj, S. Vishweswaraiah, V.H. Desai, and Y.H. Sohn, "Electrochemical Impedance Spectroscopy of Thermal Barrier Coatings as a Function of Isothermal and Cyclic Thermal Exposure," Surf. Coat. TechnoL 177-178, 140-151 (2004).

12. M. Miyata, S. Zhu, and Y. Kagawa, "Application of Microwave Self-Heating to the Detection of Microfracture in Thermal Barrier Coating System," Proc. Cer. Eng. Sci. 23 (4), 439-445.

13. X. Chen, G. Newaz, and X. Han, "Damage Assessment in Thermal Barrier Coatings using Thermal Wave Imaging Technique," ASME Int. Mech. Eng. Cong. & Expo. 66, 239-46 (2001).

14. W. A. Ellingson, J. A. Todd, and J. Sun, "Optical Method and Apparatus for Detection of Defects and Microstructural Changes in Ceramics and Ceramic Coatings," U.S. Patent 6,285,449 (2001).

15. R. J. Visher, M. D. Shields, W. A. Ellingson, and A. Feuerstein, "Laser-Based Inspection of Thermal Barrier Coatings," to be published in the Proceedings of ASM International Surface Engineering Conference 2004, ASM International, Materials Park, OH.

16. J. C. Stover, *Optical Scattering and Analysis*, SPIE Optical Engineering Press, Bellingham, Washington, pp. 111-133 (1995).

17 J. S. Steckenrider and W.A. Ellingson, "Application of Laser Scattering to the Detection of Surface and Subsurface Defects in Si_3N_4 Components," Ceram. Eng. Sci. Proc. 15(4), 382-89 (1994).

18. D.R. Clarke, J.R. Christensen, and V. Tolpygo, "The Evolution of Oxidation Stresses in Zirconia Thermal Barrier Coated Superalloy Leading to Spalling Failure," Surf. Coat. Technol., 94/95, 89-93 (1997).

19. X. Peng and D.R. Clarke, "Piezospectroscopic Analysis of Interface Debonding in Thermal Barrier Coatings," J. Am. Ceram. Soc. 83, 1165-70 (2000).

20. V. K. Topygo, D. R. Clarke, and K. S. Murphy, "Evaluation of Interface Degradation during Cyclic Oxidation of EB-PVD Thermal Barrier Coatings and Correlation with TGO Luminescence," Surf. Coat. Technol., 188-189, 62-70 (2004).

21. M. Gell, S. Sridharan, M. Wen, and E. H. Jordan, " Photoluminescence Piezospectroscopy: A Multi-Purpose Quality Control and NDI Technique for Thermal Barrier Coatings," Int. J. Applied Cer. Technol., 1(4), 316-329 (2004).

21. J. I. Eldridge, C. M. Spuckler, J. A. Nesbitt, and R. E. Martin, "Nondestructive Evaluation of Thermal Barrier Coatings by Mid-Infrared Reflectance Imaging," Cer. Eng. Sci. Proc. 26(3), 121-128 (2005).

22. R. J. Visher, L. Gast, W. A. Ellingson, and A. Feuerstein, "Health Monitoring and Life Prediction of Thermal Barrier Coatings using a Laser-based Method," ASME paper GT2005-68252 (2005).

23. P. Bengtsson, J. and Wingren, "Segmentation Cracks in Plasma Sprayed Thick Thermal Barrier Coatings," in. Proc. Gas Turbine Materials Technology, eds. P. J. Maziasz, I. G. Wright, W. J. Brindley, J. Stringer, and C. O'Brien, pp. 92-101 (1998). Published by ASM International, Materials Park, OH.

24. B. E. Bouma and G. J. Tearney, *Handbook of Optical Coherence Tomography*, Marcel Dekker, New York (2002).

25. M. Bashkansky, P.R. Battle, et al., "Subsurface Defect Detection in Ceramics Using an Optical Gated Reflectometer," J. Am. Ceram. Soc. 79(5), 1397-400 (1996).

26. A. Selcuk, and A. Atkinson, "Analysis of the Cr^{3+} Luminescence Spectra from Thermally Grown Oxide in Thermal Barrier Coatings," Mater. Sci. Eng A. 335,147-156 (2002).

27. Y. H. Sohn, K. Vaidyanathan, M. Ronski, E. H. Jordan, and M. Gell, "Thermal Cycling of EB-PVD/MCrAlY Thermal Barrier Coatings: II. Evolution of Photo-Stimulated Luminescence," Surf. Coat. Technol. 146/147,102-109 (2001).

28. T. Tomimatsu, S. Zhu, and Y. Kagawa, "Measurements of Stress Distribution in Top Coat and TGO Layers Processed by EB-PVD," Proc. Cer. Eng. Sci., 23 (4) 391-396 (2002).

29. J. Thornton, S. Slater, and J. Almer, "The Measurement of Residual Strains within Thermal Barrier Coatings Using High-Energy X-ray Diffraction," J. Am. Ceram. Soc. 88, 2817-2825 (2005).